International Journal of Innovative
Computing, Information and Control
Volume **16**, Number **1**, February **2020**

 ISSN 1349-4198
pp. 1–14

ADAPTIVE TUNING NOISE ESTIMATION FOR MEDICAL IMAGES USING MAXIMUM ELEMENT CONVOLUTION LAPLACIAN

Fung Fung Ting and Kok Swee Sim

Faculty of Engineering and Technology
Multimedia University
Jalan Ayer Keroh Lama, Bukit Beruang, Melaka 75450, Malaysia
sicily.ting@gmail.com; kssim@mmu.edu.my

Received May 2019; revised September 2019

Abstract. *Noise in medical images can adversely affect the outcome of clinical diagnosis. In analyzing medical images, noise estimation is necessary to ensure consistency and performance quality of image processing techniques. In this study, we present a noise estimation method, namely Adaptive Tuning Noise Estimation (ATNE) that implements convolution Laplacian noise estimation. ATNE is based on subtraction of Gabor wavelet detected edges of images, and involves the relation element based on the parameters of the input image. This method allows a fast estimation of the image noise variance without a heavy computational cost. To assess the effectiveness of ATNE, 1000 mammograms are used. We pre-process these images to be Rician distributed with various noise variances. ATNE is used to estimate the noise level of the resulting images. We compare ATNE with other noise estimation methods, and the results show that ATNE outperforms other related methods with a lower percentage of error for noise variance estimation.*
Keywords: Image noise estimation, Rician noise, Medical imaging, Image processing

1. **Introduction.** Noise in images poses an irregular variation of the color information, or brightness, in digital images, and it is usually a facet of electronic noise [1]. In medical image analysis, noise variance estimation is needed to ensure consistency and efficiency of image processing techniques. In addition, statistical analysis methods applied to MR (magnetic resonance) imaging often depend on prior assumptions regarding the underlying noise parameters [4,5]. Noise present in medical images may affect the diagnostic result of the patient; therefore the importance of noise reduction especially for low quality medical images. The performance of image processing methods such as image segmentation can often be improved through noise reduction. However, most of the proposed noise reduction methods are based on a predefined noise variance [4,5]. In this regard, noise estimation can provide an adaptive mechanism for many image-processing algorithms, instead of using fixed values for setting the noise levels.

Noise estimation is one of the most important factors in analyzing medical images. The effectiveness of all known image processing techniques such as image registration, segmentation, clustering, noise removal and restoration are affected by noise variance of the image [6-8]. In most cases, it is vital to be able to correctly predict the noise level in an image, in order to reduce noise effectively. When we are dealing with medical images, certain types of noise may be mistaken as brain lesion. Noisy medical images may affect the accuracy and precision of medical diagnostic outcomes.

Many methods for noise estimation have been suggested over the years. A noise estimation method that uses the Principal Component Analysis (PCA) of image blocks was

DOI: 10.24507/ijicic.16.01.1

presented [2]. This patch based method shows that the lowest eigenvalue of the image block covariance matrix can be estimated as the noise variance. It is faster and more accurate in comparison with other similar methods. The method can successfully process texture information in images, since it does not consider homogeneous areas in the image. However, patch selection does not belong to homogeneous selection; therefore, stability of the results varies. The method may cause under-estimation of the noise variance in cases containing rich texture information and high noise levels, and over-estimation in cases containing weak texture information and low noise levels.

Another patch-based method that selects the patches with the minimum standard deviation among all decomposed patches was proposed [3]. The noise level is estimated based on attributes of the selected patches. Even though the technique is efficient and simple, it is more likely to underestimate the noise variance in cases with high noise levels, and to false detect the noise level in cases with low noise levels. The reason might be the selection of image patches is relying on input images and noise level.

Furthermore, a Weak Texture Patch based Noise Estimation (WTPNE) algorithm was suggested [4,5]. The patches are produced from one noisy image. The noise variance estimation method requires the selection of image patches using the PCA and weak texture images. The algorithm is able to select low texture patches from single noisy image based on the gradient of the patches and their statistics. The noise level is estimated from the selected weak texture patches through PCA. This noise level estimation algorithm outperforms other methods. The maximum eigenvalue of the covariance matrix of the image gradient is used as the measurement metric for the strength of texture. Unlike other state-of-the-art methods, the algorithm is independent of the environment, and presents a significant improvement in accuracy and stability for a range of noise levels in different scenes. However, this method does not achieve efficient accuracy in cases of low noise levels and low texture patches.

A simple and rapid noise estimation method was presented [9]. The algorithm can be used to give a local estimate of the order differential components in the image. The algorithm uses a 3×3 mask and a summation over a local neighborhood or the image, and requires 14 integer operations per pixel. It performs well for various settings of noise variance. However, the method will considered thin lines in high texture images as noise.

A Region of Interest (ROI) based medical image compression algorithm using block-to-row bi-directional Principal Component Analysis (PCA) is introduced in [28]. The algorithm first segments the image into the ROI and the non-ROI using the segmentation method based on the level set. Then, general PCA is applied to non-ROI region whereas block-to-row bi-directional PCA is applied to ROI region in order to achieve desired image quality while improving compression ratio.

At present, effective noise estimation methods for noisy images are scarce [1]. Several reviewed methods showed drawbacks for their estimation methods [2,4,5] as mentioned in [1]. Motivated by this challenge, we design a noise estimation method using Gabor wavelet. It is based the noise estimation method in [9], with an adaptive tuning function added. This noise estimation method implements Gabor wavelet edge subtraction to pre-process noisy images. The method is applied to estimating the noise variance in medical images. By using a different parameter setting for a Gabor wavelet, other useful features pertaining to medical images can be extracted. The maximum element Convolution Laplacian is implemented on image after Gabor wavelet edge subtraction operation. This set of procedure promotes higher accuracy on noise estimation by deduction of affecting factors such as image edges and lines.

2. Problem Statement and Preliminaries.

2.1. **Rician noise.** In the work of [10], noise present in MR images belongs to the Rician Probability Distribution Function (PDF). It is not considered as additive noise, as Rician noise relies on the data. In order to add Rician noise to medical imaging, we simulate the data to be Rician distributed [11]. MR signals can be acquired at quadrature channels. An image formed by using the standard deviation of zero-mean Gaussian noise, σ_0, is used to degrade the signals. The combination of these images formed the magnitude part of the image; therefore, the Gaussian noise PDF is changed into the Rician noise PDF. We can express the joint probability density of noise as [12]

$$p(s_r, s_i) = \frac{1}{2\pi\sigma_0^2} \exp\left(-\frac{s_r^2 + s_i^2}{2\pi\sigma_0^2}\right), \tag{1}$$

where s_r is the signal of Rician distribution while s_i denotes the input image original signal.

The expected mean of the magnitude and variance can be obtained as follows [10]:

$$I = \sigma_0\sqrt{\frac{\pi}{2}} \exp\left(-\frac{X^2}{4\sigma_0^2}\right) x \left[\left(1 + \frac{X^2}{2\sigma_0^2}\right) I_0\left(\frac{X^2}{4\sigma_0^2}\right) + \frac{X^2}{2\sigma_0^2} I_1\left(\frac{X^2}{4\sigma_0^2}\right)\right], \tag{2}$$

$$\sigma_I^2 = X^2 + 2\sigma_0^2 - \frac{\pi\sigma_0^2}{2} \exp\left(\frac{X^2}{2\sigma_0^2}\right) x \left[\left(1 + \frac{X^2}{2\sigma_0^2}\right) I_0\left(\frac{X^2}{4\sigma_0^2}\right) + \frac{X^2}{2\sigma_0^2} I_1\left(\frac{X^2}{4\sigma_0^2}\right)\right], \tag{3}$$

where I_0 and I_1 are the improved Bessel functions of order 0 and 1. The function $I_1(x)/I_0(x)$ is zero at $x = 0$.

Asymmetry of the Rician distribution leads to a non-constant intensity bias, which relies on the local Signal-to-Noise Ratio (SNR). To lower such bias, one way is to remove the bias in the squared magnitude image [13].

2.2. **Gabor wavelet edge detection.** Gabor functions can be modeled as different filters, depending on the frequency and orientation settings [14]. Over the years, it has been applied to many edge detection problems (REF). The 2-D Gabor wavelet filter is actually a Gaussian kernel function, which can be regulated by a sinusoidal wave, as follows.

$$G(x, y) = \exp\left[-\frac{x^2 + y^2}{2\sigma^2}\right] \exp[j\omega(x\cos\theta + y\sin\theta)], \tag{4}$$

where σ is the Gaussian function standard deviation in the y- and x- directions, ω denotes the spatial frequency. The output of the Gabor filter $\emptyset(x, y)$ is given by:

$$\emptyset(x, y) = g(x, y) \otimes I(x, y), \tag{5}$$

where $\otimes$ defines the 2-D convolution calculation.

The Gabor wavelet reacts to the edge of an image when the edge is in perpendicular to the wavelet vector. The imaginary and real parts of $\emptyset(x, y)$ oscillate with the characteristic frequency when such an edge exists. Furthermore, the magnitude part of the filter response can produce local properties of the image effectively [15]. The convolution of the Gaussian function is represented by the Fourier transform of the impulse response of a Gabor filter. The imaginary and real components of the filter represent an orthogonal direction [16]. These components may be associated into a complex number as in Equation (6), or can be used separately as a real part as in Equation (7) or an imaginary part as in Equation (8).

Complex:

$$G(x, y; \lambda, \theta, \varphi, \sigma, \gamma) = \exp\left(-\frac{x'^2 + \gamma^2 y'^2}{2\sigma^2}\right) \exp\left(i\left(2\pi\frac{x'}{\lambda} + \varphi\right)\right), \tag{6}$$

Real:

$$(x, y; \lambda, \theta, \varphi, \sigma, \gamma) = \exp\left(-\frac{x'^2 + \gamma^2 y'^2}{2\sigma^2}\right) \cos\left(2\pi \frac{x'}{\lambda} + \varphi\right), \tag{7}$$

Imaginary:

$$(x, y; \lambda, \theta, \varphi, \sigma, \gamma) = \exp\left(-\frac{x'^2 + \gamma^2 y'^2}{2\sigma^2}\right) \sin\left(2\pi \frac{x'}{\lambda} + \varphi\right), \tag{8}$$

where, $x' = x\cos\theta + y\sin\theta$ and $y' = -x\sin\theta + y\cos\theta$, λ represents the wavelength of the sinusoidal factor, θ represents the orientation of the normal to the parallel stripes of the Gabor function, φ is the phase offset, σ is the standard deviation of the Gaussian envelope, and γ is the spatial aspect ratio, which denotes the ellipticity of the Gabor function.

The imaginary part of the Gabor filter is useful for edge detection [17]. Mostly, a group of $U \times V$ Gabor wavelets is needed to perform multi-orientation and multi-resolution analyses.

$$\begin{aligned} &\left\{\varphi_{discrete(f_u,\theta_v,\gamma,n)}(x, y)\right\}, \\ &f_u = \frac{f_{\max}}{\sqrt[u]{2}}, \\ &\theta_v = \frac{v}{V}\pi, \quad u = 0, \ldots, U-1, \quad v = 0, \ldots, V-1, \end{aligned} \tag{9}$$

where θ_v and f_u denote the scale and orientation of a Gabor wavelet, $f_{\max}$ is the maximum central frequency while the factor of spacing among different central frequencies is 2. Figure 1 shows a Gabor wavelet with 8 different orientations and 4 different scales.

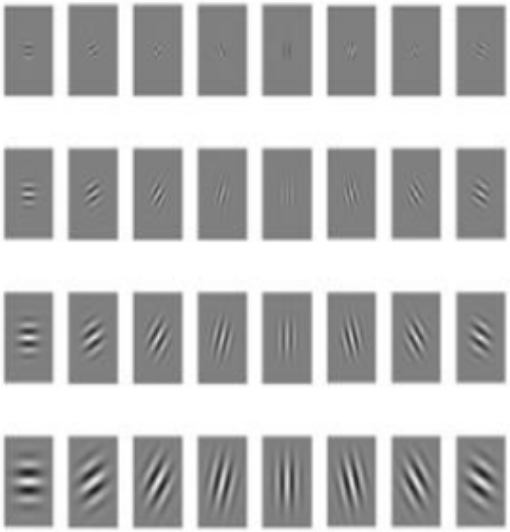

FIGURE 1. The real part of a Gabor wavelet with 8 different orientations and 4 distinct scales [18]

By using a different parameter setting for a Gabor wavelet, other useful features pertaining to medical images can be extracted.

2.3. **Fast Noise Variance Estimation using Convolution of the Laplacian operator (FNVECL).** The Fast Noise Variance Estimation using Convolution of the Laplacian operator (FNVECL) was introduced as a fast and simple noise variance estimation method based on the Laplacian operator [9]. Figure 2 shows the flow of the method.

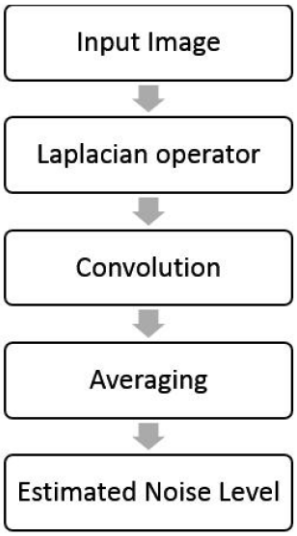

FIGURE 2. The flow of fast noise variance estimation [9]

According to Figure 2, input image is processed through Laplacian operator. Then the processed image matrix is processed through convolutional operation. Convolution operates on two signals (in 1D) or two images (in 2D). In 2 dimensional practice, "input" signal may refer to image, and the other (called the kernel) as a "filter" on the input image, producing an output image. Hence, convolution takes two images as input and produces a third as output. Averaging operation is applied to reduce the density of intensity variation between neighboring pixels with integral image method. Each output pixel contains the mean value of the 3-by-3 neighborhood around the corresponding pixel in the input image. As suggested in [6], a noise estimator should be insensitive to the Laplacian of an image, since the image structures such as edges have strong second order differential components. The difference between two masks, M_1 and M_2 is applied to the noise estimation operator, N, as in (12) [9].

The elements of M_1 and M_2 are

$$M_1 = \begin{bmatrix} 0 & 1 & 0 \\ 1 & -4 & 1 \\ 0 & 1 & 0 \end{bmatrix}, \tag{10}$$

$$M_2 = \frac{1}{2}\begin{bmatrix} 1 & 0 & 1 \\ 0 & -4 & 0 \\ 1 & 0 & 1 \end{bmatrix}. \tag{11}$$

The noise estimation operator N is the mask operation:

$$N = 2(M_2 - M_1)\begin{bmatrix} 1 & -2 & 1 \\ -2 & 4 & -2 \\ 1 & -2 & 1 \end{bmatrix}, \tag{12}$$

which has zero mean and variance by assuming that every noise has a standard deviation of σ_n.

Let $I(x, y) * N$ represent the value of applying mask N at position (x, y) in image I.

By calculating the output variance of the N operator that is applied to image I, an estimate of $36\sigma_n^2$ at every pixel is produced, which can be averaged over a local neighbourhood or the entire image to provide an estimate of the noise level, σ_n^2. The standard

deviation of the noise variance can be calculated as follows

$$\sigma_n = \sqrt{\frac{\pi}{2}} \frac{1}{6(W-2)(H-2)} \Sigma_{image\ I} |I(x,y) * N|, \tag{13}$$

where W and H are the width and height of an image, respectively.

Since there is no complex calculation involved in this method, it can produce the estimated noise in a fast manner. This calculation uses one multiplication for an estimate of the noise variance per pixel. This may lead to detecting lines as noise, and affect the estimated noise level. As a result, we propose to include an edge detector to subtract the detected edge lines from the image, in order to enhance the performance of the noise estimation method in [9].

2.4. **Adaptive Tuning Noise Estimation.** Adaptive Tuning Noise Estimation (ATNE) is implemented based on the fast noise variance estimation method in [6], with improvement to the algorithm. Firstly, assume that the images are corrupted with noise by making it Rician distributed. Then, perform edge detection on the images by using the Gabor wavelet due to its adaptability. The Gabor wavelet parameters are set to 1 scale and 8 orientations for fast computation. Once the Gabor kernel based on the preset parameter is obtained, it is used to filter the Rician distributed images, and to produce the edge map. The acquired edge map is subtracted from the original image. The edge map generated by the Gabor wavelet is applied to subtracting unnecessary lines and edges in the noisy images. The edge lines of the images may influence the accuracy of noise estimation. So, it should be excluded in order to achieve robust noise variance estimation.

We assume that there is a relation element between noise free images and noisy images. This relation element is studied using 1000 DICOM images with different simulated Rician noise variances, ranging from 0.01 to 0.20. Specifically, an image can be expressed in term of an $m \times n$ matrix, as follows.

$$Image, I = \begin{bmatrix} a_{11} & \cdots & a_{1n} \\ \vdots & \ddots & \vdots \\ a_{m1} & \cdots & a_{mn} \end{bmatrix} = \begin{pmatrix} a_{11} & \cdots & a_{1n} \\ \vdots & \ddots & \vdots \\ a_{m1} & \cdots & a_{mn} \end{pmatrix} = (a_{ij}) \in \mathrm{R}^{m \times n}. \tag{14}$$

The global maximum element is identified from the whole image matrix. The maximum elements of both noise-free and noisy images are plotted. Through the graphs of 1000 CT images, we can observe a linear relationship, as shown in Figure 3.

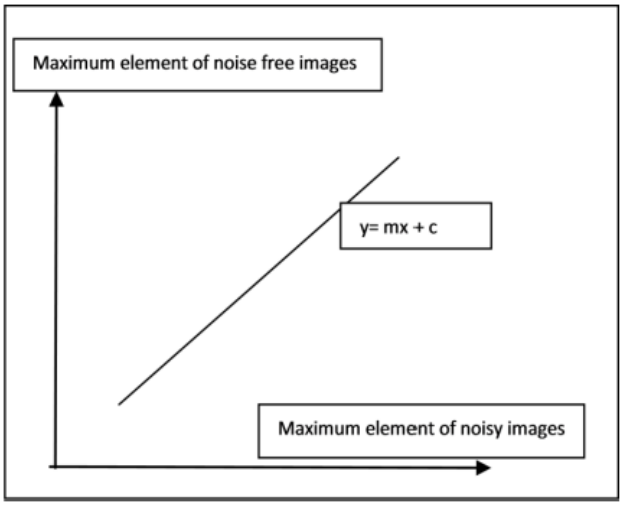

FIGURE 3. A linear trend for the maximum elements of noise-free and noisy images

From the experimental results, we notice that the slope and y-intercept change, respectively. We compute the relation element and substitute it into our noise estimation equation, as follows

$$\sigma_n = \sqrt{\frac{\pi}{2}} \frac{1}{6(W-2)(H-2)} \Sigma_{image\ I} |I(x,y) * N|, \tag{15}$$

$$\sigma_{ATNE} = \frac{\sigma_n}{\tilde{R}^3}, \tag{16}$$

where $\tilde{R}^3$ is the third iterated relation element,

$$\sigma_{ATNE} = \sqrt{\frac{\pi}{2}} \frac{1}{6(W-2)(H-2)\left(\tilde{R}^3\right)} \Sigma_{image\ I} |I(x,y) * N|. \tag{17}$$

The adjusted noise estimation shown in (17) is employed on the edge-subtracted image to estimate the noise variance present in the image. ATNE is adaptive to the input image values, and can provide robust and rapid noise estimation. Figure 4 shows a block diagram of our proposed method.

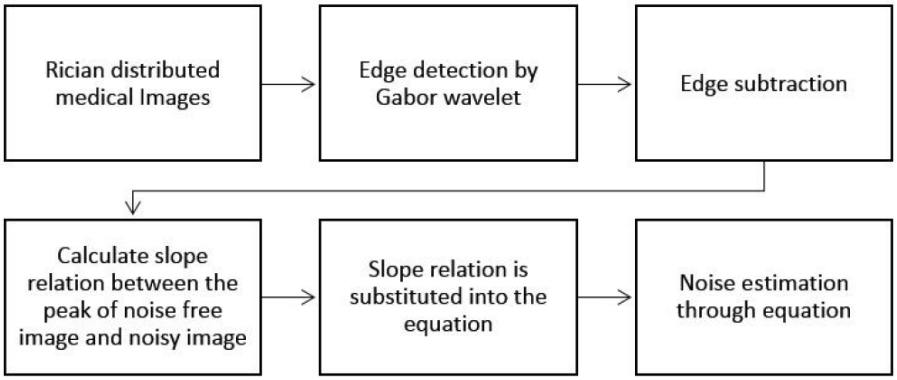

FIGURE 4. The block diagram of our method

2.5. **Adaptive Tuning Fast Nonlocal Mean Denoise Filter (ATFNLM).** The estimated noise variance obtained from ATNE is used in Adaptive Tuning Fast Nonlocal Mean Denoise Filter (ATFNLM) for medical images denoise purpose. Adaptive estimation of noise variances allows accurate and practical application of image denoise filters.

Nonlocal Means (NLM) is defined as the nonlinear filter, which depends on a Weighted Average (WA) of pixels inside a relatively large search window. The pixels within the search window are weighted according to their similarity with the pixel of interest to sustain the structures of the image [19-21]. The nonlocal means denoising presented practical result for filtering out noisy medical images [19-21]. NLM had been improved and suggested for different medical imaging methods [22,23].

NLM computation can be expressed in the following mathematical equations.

Generally, $u(x_i)$ represents the pixel at position x_i and the filtered output is calculated as in Equation (18)

$$\hat{u}(x_i) = \Sigma_{x_j \in \Omega_i} w(x_i, x_j) u(x_j), \tag{18}$$

where Ω_i represents the large search window centred at pixel x_i and the weight $w(x_i, x_j)$ is assigned from x_j to pixel x_i. This assignment is referring to the similarity between two patches N_i and N_j centred at x_i and x_j respectively:

$$w(x_i, x_j) = \frac{1}{z} \exp\left(-\frac{d(x_i, x_j)}{h^2}\right), \tag{19}$$

$$d(x_i, x_j) = \frac{1}{N}\|u(N_i) - u(N_j)\|_2^2, \tag{20}$$

where z denotes a normalizing constant, so that $\Sigma_{x_j} w(x_i, x_j) = 1$, and $u(N_i)$ defines $N \times 1$ vector with values $u(x_i)$ around the pixels $x_j \in N_i$. The parameter h needs to be proportional to the estimated distance value between patches $\{d(x_i, x_j)\}$. Thus, it is relevant to the noise variance of the image, σ^2. Basically, it is suggested to set the parameter to $h^2 = \beta^2\sigma^2$ for $\beta \in [0.8, 1.2]$ [22,23]. The distance between batches is required to estimate correctly. NLM might over smooth the image's structures of interest if $E\{d(x_i, x_j)\}$ is over estimated. NLM may not properly filter the noise in the image if the $E\{d(x_i, x_j)\}$ is underestimated.

There are enormous computation loads involved in the Equations (19) and (20). This remains as the disadvantage of NLM. Numerous efforts had been carried out to improve the computational load of NLM. The suggested approach had been applied to this filter. The computation of patch distances $d(x_i, x_j)$ is reduced to a small subset feature for all pixels $x_j \in \Omega_i$. This can decrease the computational load for NLM. The quadratic differences between every pair of respective pixels are relying on its physical distance to the centre of the patch N_i:

$$d(x_i, x_j) = (u_i - u_j)^T R(u_i - u_j), \tag{21}$$

where R is a diagonal matrix that is corresponding to the n-dimensional kernel applied to regulate the distances. By considering the weighting kernel, the quadratic differences are calculated as shown in Equation (22):

$$\bar{u} = \Sigma_{x_j \in N_i} \rho_j u(x_j) = I_{N\times 1}^T Ru; \quad \Sigma_{x_j \in N_i} \rho_j = 1, \tag{22}$$

where 1 represents an $N \times 1$ vector comprising of all ones and ρ_j denotes the value of the multivariate kernel at every pixel location $x_j \in N_i$. In case if the kernel is separable, then all local averages can be calculated as separable convolutions. By particularizing the kernel to the condition $\rho_j = 1/N$, the unweighted patch distance is expressed as in Equation (23):

$$E\left\{\tilde{d}(x_i, x_j)\right\} = u\left(RX\left(X^T X\right)^{-1} X^T\right) \bullet E\{d(x_i, x_j)\}. \tag{23}$$

Hence, the effective value of h that is used as the range for small patch distance is as shown in Equation (24):

$$h_{eff}^2 = u\left(RX\left(X^T X\right)^{-1} X^T\right) \bullet h^2. \tag{24}$$

This value can determine the barrier of patch distance fallout from this value range would not be considered as in the NLM search window. This will decrease the computational cost of the searching procedures for NLM thus improve the time taken for NLM filtering process. The ATFNLM filters the noisy medical images to enhance the image quality to aid medical experts in diagnosis process.

3. **Main Results.** To illustrate the performance of the proposed ATNE method on medical images, different datasets of medical images were applied. 1000 mammograms were used in the experiment to compare the noise estimation performance between Weak Texture Patch based Noise Estimation (WTPNE) [5], Fast Noise Variance Estimation through Convolution of Laplacian operator (FNVECL) [9] and Adaptive Tuning Noise Estimation (ATNE). The performance evaluation between mentioned methods of noise estimation was done on 1000. We processed 1000 medical images to be Rician distributed with various noise variances, which vary from 0.01 to 0.20 according to standard range of noise variance. Later on, ATNE was used to estimate the noise level of those medical images.

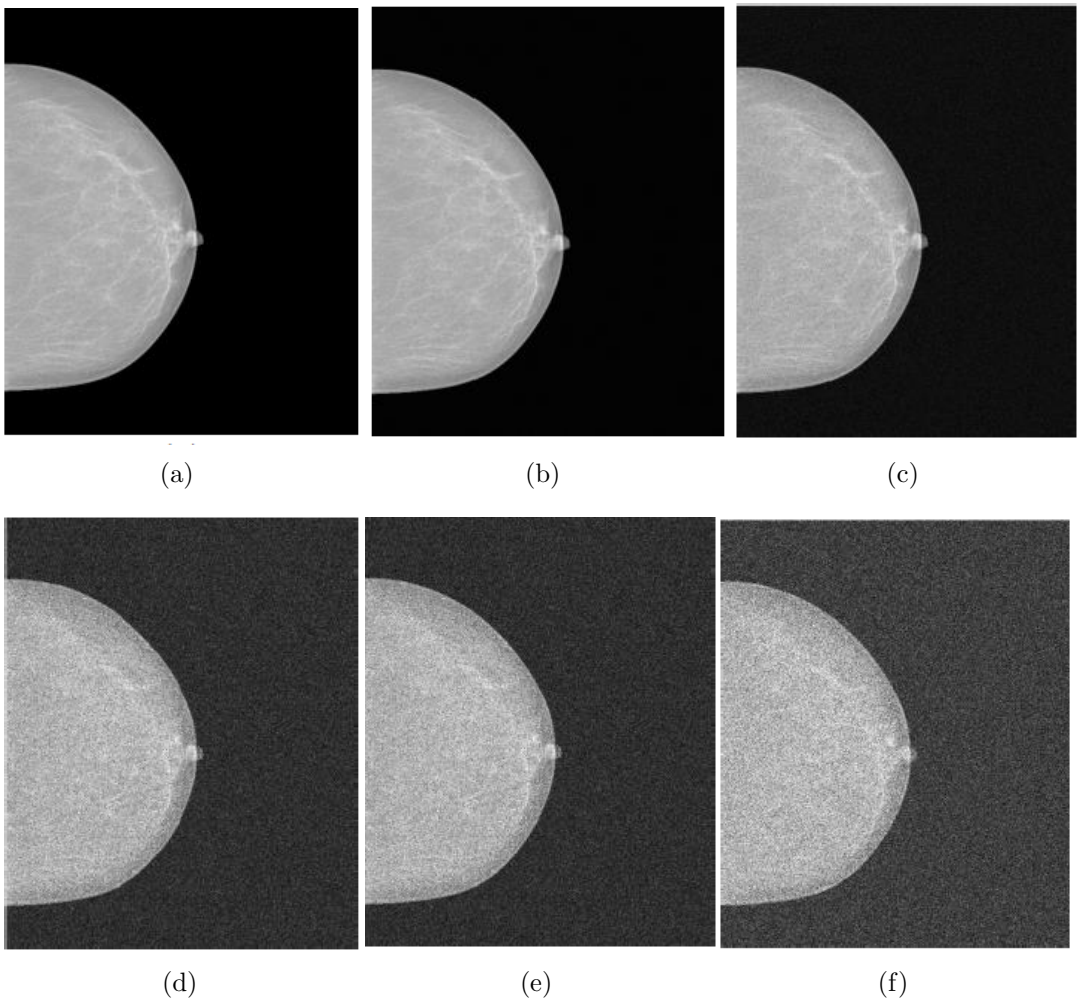

(a) (b) (c)

(d) (e) (f)

FIGURE 5. The Rician distributed mammogram with different noise variance added. (a) Original mammogram; (b) added noise variance is 0.01; (c) added noise variance is 0.05; (d) added noise variance is 0.10; (e) added noise variance is 0.15; (f) added noise variance is 0.20.

To illustrate the performance of the proposed ATNE technique, Figure 5 shows the Rician distributed images with noise variance, $\sigma = 0.01, 0.05, 0.10, 0.15, 0.20$, as well as the original image.

The percentage error is used as the performance metric for FNVECL [9], WTPNE [5] and ATNE, as follows.

$$Percentage\ Error = \frac{|\sigma_{estimated} - \sigma_{added}|}{\sigma_{added}} \times 100. \tag{25}$$

Table 1 shows the performance comparison among FNVECL [9], WTPNE [5], and ATNE on one selected CT image in Figure 5. The bolded results indicate ATNE is able to achieve mostly the smallest percentage error rates, i.e., better estimation of the noise ratio. Our method maintains a good performance for various noise levels. However, FNVECL [9], WTPNE [5], perform poorly in cases with high noise variance. Table 1 shows the overall performance comparison on 1000 mammograms. ATNE outperforms other methods by producing consistent results on the estimated noise variance, since its results are close to reference noise variances. FNVECL [9], WTPNE [5] produce results

TABLE 1. The comparison of noise estimation methods for 1000 mammograms

σ_{added}	FNVECL [9]	WTPNE [5]	ATNE
	PE, %	PE, %	PE, %
0.01	16.3685	32.8642	**16.0801**
0.02	20.3669	29.3230	**20.1113**
0.03	21.6280	27.2141	**21.3818**
0.04	21.9799	25.7375	**21.7389**
0.05	22.2941	25.2151	**22.0560**
0.06	22.5362	24.9717	**22.2998**
0.07	22.7352	24.8967	**22.5000**
0.08	22.9013	24.8905	**22.6672**
0.09	23.0510	24.9117	**22.8177**
0.10	23.2166	24.9621	**22.9842**
0.11	23.3651	25.0421	**23.1331**
0.12	23.5182	25.1047	**23.2869**
0.13	23.6718	25.2037	**23.4407**
0.14	23.8232	25.3053	**23.5927**
0.15	23.9799	25.4198	**23.7498**
0.16	24.1571	25.5385	**23.9276**
0.17	24.3251	25.6739	**24.0959**
0.18	24.5030	25.7944	**24.2744**
0.19	24.6813	25.9469	**24.4527**
0.20	24.8608	26.0960	**24.6326**

that stray from the reference noise variances. Both methods perform poorly on images with high noise variances.

Table 1 shows the comparison of percentage error for 1000 mammograms. The tabulated data showed that ATNE outperforms WTPNE and FNVECL in terms of having the smallest percentage error in noise estimation and consistent good performance for various noise variances. Moreover, ATNE has the most consistent performance on noise estimation in various noise levels.

3.1. **Discussion on Adaptive Tuning Fast Nonlocal Mean Denoise Filter (ATFNLM).** The estimated noise variance obtained from ATNE is used in Adaptive Tuning Fast Nonlocal Mean Denoise Filter (ATFNLM) to denoise the medical images. Nonlocal Means (NLM) are defined as the nonlinear filter which relies on a Weighted Average (WA) of pixels inside a relatively large search window.

The Mean Squared Error (MSE), Root-Mean-Squared Deviation (RMSD) and the Structural Similarity (SSIM) index are applied as the image quality measurement metrics. These image quality measurement metrics are used to evaluate the performance of Adaptive Tuning Fast Nonlocal Mean Denoise Filter (ATFNLM) against other existing methods such as Adaptive Nonlocal Mean Filter (ANMF), and Improved Nonlocal Mean Filter (INLM).

The Mean Squared Error (MSE) is computed using Equation (26).

$$Mean\,Squared\,Error\,(MSE) = \frac{\Sigma_{i,j}\left(I_{filtered}(i,j) - I_{reference}(i,j)\right)^2}{N}, \tag{26}$$

where $I_{filtered}(i,j)$ represents the filtered image and $I_{reference}(i,j)$ represents the reference input image. In our case, the MSE denoted the mean value of the squared difference

between filtered image and reference image. The lower the MSE value the closer it is to the reference image, which indicates a good performed image filter.

The Root-Mean-Squared Deviation (RMSD) is commonly used as the measurement of the differences between predicted values and actual value. In our circumstances, RMSD is used to compute the difference between the filtered image and reference image. RMSD is calculated through Equation (27).

$$\begin{aligned} &Root\text{-}Mean\text{-}Squared\ Deviation\ (RMSD) \\ &= \sqrt{MSE} = \sqrt{\frac{\Sigma_{i,j}\left(I_{filtered}(i,j) - I_{reference}(i,j)\right)^2}{N}}, \end{aligned} \tag{27}$$

where smaller RMSD value indicates closer distance between $I_{filtered}(i,j)$ and $I_{reference}(i,j)$.

The Structural Similarity (SSIM) index is often used to measure the similarity between two images. The SSIM measures image quality based on an initial distortion-free image as reference image. The computation of SSIM index is based upon three terms, such as luminance term, the contrast term, and the structural term. The multiplicative combination of these three terms represents the overall SSIM index. The SSIM index is computed as shown in Equation (28).

$$Structural\ Similarity\ Index,\ SSIM(x,y) = [l(x,y)]^{\alpha} \cdot [c(x,y)]^{\beta} \cdot [s(x,y)]^{\gamma}, \tag{28}$$

where the luminance term $l(x,y)$, contrast term $c(x,y)$, and the structural term $s(x,y)$ are shown in Equations (29), (30), and (31).

$$Luminance\ term,\ l(x,y) = \frac{2\mu_x\mu_y + c_1}{\mu_x^2 + \mu_y^2 + c_1}, \tag{29}$$

$$Contrast\ term,\ c(x,y) = \frac{2\sigma_x\sigma_y + c_2}{\sigma_x^2 + \sigma_y^2 + c_2}, \tag{30}$$

$$Structural\ term,\ s(x,y) = \frac{\sigma_{xy} + c_3}{\sigma_x\sigma_y + c_3}, \tag{31}$$

where μ_x, μ_y, σ_x, σ_y, and σ_{xy} are the local means, standard deviations, and cross covariance for images x, y. Given if $\alpha = \beta = \gamma = 1$ and $c_3 = c_2/2$, the SSIM index is simplified as:

$$SSIM(x,y) = \frac{(2\mu_x\mu_y + c_1)(2\sigma_{xy} + c_2)}{(\mu_x^2 + \mu_y^2 + c_1)(\sigma_x^2 + \sigma_y^2 + c_2)}. \tag{32}$$

The input image or reference image, noisy image and filtered images are shown in Figure 6.

The Adaptive Tuning Fast Nonlocal Mean Denoise Filter (ATFNLM) was designed by using the Adaptive Tuning Noise Estimation (ATNE) to estimate the noise in medical images as input. Then, the image noise was filtered. We are able to obtain satisfying results in comparison to other existing filter methods such as by Median Filter [24], Joint Bilateral Filter [25] and Improved Gaussian Filter [26]. We suggest reducing the size of the search window and adjusting the similarity window to decrease the computation cost of the filter operation.

According to Figure 6, IMF, JBF, IGF and ATFNLM filter the noisy image. By visual inspection, the image filtered by our ATFNLM is closer to original mammogram. The performance comparison between these filters is as shown in Table 2.

Table 2 showed that our Adaptive Tuning Fast Nonlocal Mean Denoise Filter (ATFNLM) outperforms other nonlocal mean filters techniques by having closer index values to the reference images. The average RMSE, PSNR and SSIM index for Improved Median Filter (IMF) [24] are 0.0564, 26.5036, and 0.2982 respectively. Moreover, the average

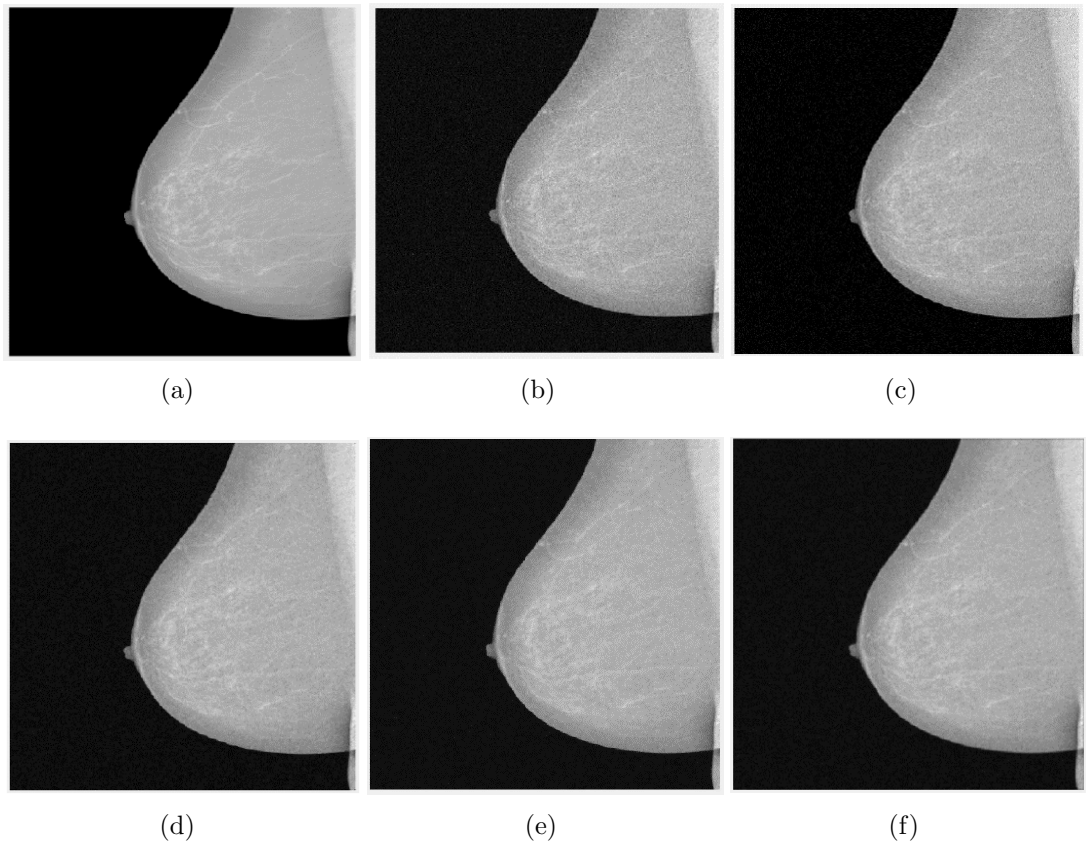

(a) (b) (c)

(d) (e) (f)

FIGURE 6. The input image, noisy image and filtered images. (a) Original CT image; (b) noisy image with noise variance = 5%, $\boldsymbol{\sigma_{added}} = 0.05$; (c) filtered image by Adaptive Tuning Fast Nonlocal Mean Denoise Filter (ATFNLM); (d) filtered image by Improved Median Filter (IMF) [24]; (e) filtered image by Joint Bilateral Filter (JBF) [25] with SSIM = 0.7397; (f) filtered image by Improved Gaussian Filter (IGF) [26].

TABLE 2. The comparison between IMF, JBF, IGF and ATFNLM on mammograms

$\boldsymbol{\sigma_{added}}$	Improved Median Filter (IMF) [24]			Joint Bilateral Filter [25]			Improved Gaussian Filter [26]			ATFNLM		
	RMSE	**PSNR**	**SSIM**	**RMSE**	**PSNR**	**SSIM**	**RMSE**	**PSNR**	**SSIM**	**RMSE**	**PSNR**	**SSIM**
0.01	0.00	38.666	0.596	0.013	37.991	0.575	0.015	36.260	0.574	0.009	57.670	**0.792**
0.02	0.019	33.448	0.409	0.022	33.134	0.405	0.024	32.425	0.401	0.019	53.250	**0.503**
0.03	0.029	30.109	0.342	0.032	29.882	0.353	0.034	29.483	0.343	0.029	48.955	**0.401**
0.04	0.031	27.680	0.304	0.042	27.487	0.327	0.044	27.212	0.312	0.031	46.288	**0.370**
0.05	0.039	25.776	0.275	0.053	25.549	0.308	0.054	25.383	0.289	0.039	44.530	**0.357**
0.06	0.047	24.211	0.251	0.063	24.040	0.291	0.064	23.861	0.270	0.047	43.238	**0.322**
0.07	0.068	22.883	0.229	0.073	22.714	0.274	0.075	22.559	0.251	0.068	42.159	**0.294**
0.08	0.096	21.731	0.209	0.084	21.560	0.254	0.085	21.422	0.234	0.096	41.132	**0.275**
0.09	0.111	20.712	0.191	0.094	20.536	0.233	0.096	20.414	0.219	0.111	40.083	**0.263**
0.10	0.124	19.820	0.176	0.104	19.636	0.212	0.106	19.531	0.205	0.124	38.990	**0.251**
$^*\boldsymbol{\sigma_{added}}$ = Added noise												

RMSE, PSNR, and SSIM index for Joint Bilateral Filter [25] are 0.058, 26.2529, and 0.3232 accordingly. The average RMSE, PSNR, and SSIM index for our previous Improved Gaussian Filter [26] are 0.0597, 25.855, and 0.3098 accordingly. Whereby, the average RMSE, PSNR, and SSIM index for our Adaptive Tuning Fast Nonlocal Mean Denoise Filter (ATFNLM) are 0.0573, 45.6295, and 0.3828 respectively. This indicates our ATFNLM has the best performance among these filters. Furthermore, ATFNLM filtered the medical imaging through Adaptive Tuning Noise Estimation (ATNE) to reduce the chance of over smoothing the medical images. This is to decrease the chances of affecting the image quality through filtering.

4. **Conclusion.** In conclusion, we present our proposed method which is an improved noise estimation algorithm based on the FNVECL [6]. We have adapted the noise variance estimation method and implemented by adding the maximum relation element and including Gabor wavelet for edge subtraction. Thus, it is able to exclude the detected edges of medical images in order to perform more precise noise variance estimation and adjustable through different data sets. Our method shows improved performance upon FNVECL [9] and WTPNE [5]. The presented work is only experimented on mammograms. Various types of medical images can be served as input images for this presented method. This method can be further implemented by adjusting the parameter setting of the Gabor wavelet edge detector and implement the learning capability of neural networks to increase the reliability of the noise estimator. Based on the good performs noise estimator, we can design an adaptive denoise filter to further enhance the medical image quality to aid radiologist and medical experts in their practical works.

Acknowledgement. We would like to acknowledge Mammographic Image Analysis Society (MIAS) [27] for providing the real patient digital mammogram dataset. Fundamental Research Grant Scheme (FRGS) funds this research; it is a research grant from the Ministry of Higher Education (MOHE), Malaysia.

REFERENCES

[1] B. P. Ram and S. Choudhary, Survey paper on different approaches for noise level estimation and denoising of an image, *International Journal of Science and Research (IJSR)*, vol.3, no.4, pp.618-622, Available: http://www.ijsr.net/archive/v3i4/MDIwMTMxNTQ2.pdf, 2014.

[2] S. Pyatykh, J. Hesser and L. Zheng, Image noise level estimation by principal component analysis, *IEEE Trans. Image Processing*, vol.22, no.2, pp.687-699, Available: http://ieeexplore.ieee.org/stamp/stamp.jsp?tp=&arnumber=6316174&isnumber=6407512, 2013.

[3] D. H. Shin, R. H. Park, S. Yang and J. H. Jung, Block-based noise estimation using adaptive Gaussian filtering, *IEEE Trans. Consumer Electronics*, vol.51, no.1, pp.218-226, 2005.

[4] X. Liu, M. Tanaka and M. Okutomi, Noise level estimation using weak textured patches of a single noisy image, *The 19th IEEE International Conference on Image Processing*, Available: http://ieeexplore.ieee.org/stamp/stamp.jsp?tp=&arnumber=6466947&isnumber=6466779, 2012.

[5] X. Liu, M. Tanaka and M. Okutomi, Single-image noise level estimation for blind denoising, *IEEE Trans. Image Processing*, vol.22, no.12, pp.5226-5237, Available: http://ieeexplore.ieee.org/stamp/stamp.jsp?arnumber=6607209, 2013.

[6] R. B. Jeyavathana, B. Ramasamy and A. Pandian, A survey: Analysis on pre-processing and segmentation techniques for medical images, *International Journal of Research and Scientific Innovation (IJRSI)*, 2016.

[7] Z. Xu, M. Gao, G. Z. Papadakis, B. Luna, S. Jain, D. J. Mollura and U. Bagci, Joint solution for PET image segmentation, denoising, and partial volume correction, *Medical Image Analysis*, vol.46, pp.229-243, doi: 10.1016/j.media.2018.03.007, 2018.

[8] G. Chen, P. Zhang, Y. F. Wu, D. Shen and P. T. Yap, Denoising magnetic resonance images using collaborative non-local means, *Neurocomputing*, vol.177, pp.215-227, doi: 10.1016/j.neucom.2015.11.031, 2016.

[9] J. Immerker, Fast noise variance estimation, *Computer Vision and Image Understanding*, vol.64, no.2, pp.300-302, Available: http://www.sciencedirect.com/science/article/pii/S1077314296900600, 1996.
[10] H. Gudbjartsson and S. Patz, The Rician distribution of noisy MRI data, *Magnetic Resonance in Medicine: Official Journal of the Society of Magnetic Resonance in Medicine*, vol.34, no.6, pp.910-914, 1995.
[11] C. G. Koay and P. J. Besser, Analytically exact correction scheme for signal extraction from noisy magnitude MR signals, *Journal of Magnetic Resonance*, vol.179, pp.317-322, 2006.
[12] G. H. Cottet and L. Germain, Image processing through reaction combined with nonlinear diffusion, *Mathematics of Computation*, vol.61, no.204, pp.659-673, 1993.
[13] N. Wiest-Daessle, S. Prima, P. Coupe, S. P. Morrissey and C. Barillot, Rician noise removal by non-local means filtering for low signal-to-noise ratio MRI: Applications to DT-MRI, *Med. Image. Comput. Assist. Interv.*, vol.11, pp.171-179, Available: http://www.ncbi.nlm.nih.gov/pubmed/18982603, 2008.
[14] B. S. Manjunath and W. Y. Ma, Texture features for browsing and retrieval of image data, *IEEE Trans. Pattern Anal. Mach. Intell.*, vol.18, no.8, pp.837-842, 1996.
[15] R. Mehrotra, K. R. Namuduri and N. Ranganthan, Gabor filter-based edge detection, *Pattern Recognition*, vol.25, no.12, pp.1479-1494, Available: http://www.sciencedirect.com/science/article/pii/003132039290121X, 1992.
[16] J. J. Henriksen, *3D Surface Tracking and Approximation Using Gabor Filters*, Syddansk Universitet, 2007.
[17] F. Pellegrino, W. Vanzella and V. Torre, Edge detection revisited, *IEEE Trans. Systems, Man, and Cybernetics*, vol.34, no.3, pp.1500-1518, 2004.
[18] L. Shen and L. Bai, A review of Gabor wavelets for face recognition, *Pattern Analysis Application*, vol.9, pp.273-292, 2006.
[19] A. Buades, B. Coll and J. M. Morel, Image denoising methods. A new nonlocal principle, *SIAM Review*, http://doi.org/10.1137/090773908, 2010.
[20] A. Buades, B. Coll and J. M. Morel, Nonlocal image and movie denoising, *International Journal of Computer Vision*, http://doi.org/10.1007/s11263-007-0052-1, 2008.
[21] A. Buades, B. Coll and J. M. Morel, Non-local means denoising, *Image Processing On Line*, http://doi.org/10.5201/ipol.2011.bcm_nlm, 2011.
[22] J. V. Manjón, P. Coupé and A. Buades, MRI noise estimation and denoising using non-local PCA, *Medical Image Analysis*, http://doi.org/10.1016/j.media.2015.01.004, 2015.
[23] J. V. Manjón, P. Coupé, L. Concha, A. Buades, D. L. Collins and M. Robles, Diffusion weighted image denoising using overcomplete local PCA, *PLoS ONE*, http://doi.org/10.1371/journal.pone.0073021, 2013.
[24] A. H. H. Alasadi and A. K. H. Al-Saedi, A method for microcalcifications detection in breast mammograms, *Journal of Medical Systems*, http://doi.org/10.1007/s10916-017-0714-7, 2017.
[25] A. Mahmoud, Joint bilateral filter, https://www.mathworks.com/matlabcentral/fileexchange/62455-joint-bilateral-filter, MATLAB Central File Exchange, Retrieved April 8, 2019.
[26] M. Kaur, S. Gupta and B. Bhushan, An improved adaptive bilateral filter to remove Gaussian noise from color images, *International Journal of Signal Processing, Image Processing and Pattern Recognition*, http://doi.org/10.14257/ijsip.2015.8.3.05, 2015.
[27] J. Suckling, J. Parker and D. Dance, The mammographic image analysis society digital mammogram database, *Exerpta Medica, International Congress Series*, 1994.
[28] Z. Fan, X. Rong and X. Yu, Region of interest based medical image compression using block-to-row bi-directional principal component analysis, *ICIC Express Letters*, vol.11, no.12, pp.1765-1772, 2017.